Benign-by-Design: Synthesis of Engineered Silicon Nanoparticles and their Application to Oil Sands Water Contaminant Remediation

Muhammad Iqbal, Tapas K. Purkait, Jonathan G.C. Veinot

Department of Chemistry, University of Alberta

Greg G. Goss

Department of Biological Sciences, University of Alberta

November 2013

Oil Sands Research and Information Network

The Oil Sands Research and Information Network (OSRIN) is a university-based, independent organization that compiles, interprets and analyses available knowledge about managing the environmental impacts to landscapes and water impacted by oil sands mining and gets that knowledge into the hands of those who can use it to drive breakthrough improvements in regulations and practices. OSRIN is a project of the University of Alberta's School of Energy and the Environment (SEE). OSRIN was launched with a start-up grant of $4.5 million from Alberta Environment and a $250,000 grant from the Canada School of Energy and Environment Ltd.

OSRIN provides:

- **Governments** with the independent, objective, and credible information and analysis required to put appropriate regulatory and policy frameworks in place
- **Media, opinion leaders and the general public** with the facts about oil sands development, its environmental and social impacts, and landscape/water reclamation activities – so that public dialogue and policy is informed by solid evidence
- **Industry** with ready access to an integrated view of research that will help them make and execute environmental management plans – a view that crosses disciplines and organizational boundaries

OSRIN recognizes that much research has been done in these areas by a variety of players over 40 years of oil sands development. OSRIN synthesizes this collective knowledge and presents it in a form that allows others to use it to solve pressing problems.

Citation

This report may be cited as:

Iqbal, M., T.K. Purkait, J.G.C. Veinot and G.G. Goss, 2013. Benign-by-Design: Synthesis of Engineered Silicon Nanoparticles and their Application to Oil Sands Water Contaminant Remediation. Oil Sands Research and Information Network, University of Alberta, School of Energy and the Environment, Edmonton, Alberta. OSRIN Report No. TR-42. 30 pp.

Copies of this report may be obtained from OSRIN at osrin@ualberta.ca or through the OSRIN website at http://www.osrin.ualberta.ca/en/OSRINPublications.aspx or directly from the University of Alberta's Education & Research Archive at http://hdl.handle.net/10402/era.17507.

Table of Contents

LIST OF TABLES

LIST OF FIGURES

REPORT SUMMARY

Oil sands are naturally occurring mixtures of sand or clay, water, fine silts, and bitumen. The oil sands extraction process consumes large volumes of water (i.e., *ca.* 3 barrels of fresh water for every 1 barrel of oil). Following the extraction of bitumen from the oil sands, a tailings slurry is produced that consists of oil sands process-affected water (OSPW), sand, silt, clay particles and trace quantities of unrecovered bitumen. This slurry is hydraulically transported to large containment facilities (i.e., open tailings ponds) that, in Alberta, currently occupy approximately 130 km^2 with 200 million litres of mature fine tailings produced each day. These vast storage facilities pose a risk to the environment, wildlife, and society.

There are many candidate technologies that could be applied to the treatment of OSPW. Advanced oxidation processes (AOPs) are particularly useful for degrading biologically toxic or non-degradable materials such as aromatics, pesticides, petroleum constituents, and volatile organic compounds in wastewater.

In this report, we investigate the use of advanced oxidation processes via photocatalysts based on nanoparticles. Silicon nanoparticles were specifically engineered for water remediation by making them water soluble and more potent towards contaminant removal. Si nanoparticles of different sizes and morphologies were investigated for model contaminant (methanol) removal in the presence of UV light. A medium pressure UV lamp was used for the purpose. Control experiments were also performed to ascertain the extent of remediation by the Si nanoparticles. Effect of methanol concentration, nanoparticle concentration and exposure time of UV were systematically studied to optimize the remediation parameters. Moreover, a cost effective and high yielding synthetic protocol was also developed for large scale synthesis of Si nanoparticles which is crucial for scale up. Quantum yield calculations were performed on different Si nanoparticles and compared with titanium dioxide (TiO_2), the most commonly proposed nanoparticle system.

ACKNOWLEDGEMENTS

The Oil Sands Research and Information Network (OSRIN), School of Energy and the Environment (SEE), University of Alberta and the Canada School of Energy and Environment Ltd. provided funding for this project.

The authors would like to thank Dr. James R. Bolton for insightful discussions on quantum yield calculations of nanoparticles. We would also like to thank Wayne Moffat, Greg Popowich and Nathan Gerein for assistance with FT-IR, TEM and SEM measurements respectively.

1 INTRODUCTION

Detrimental anthropogenic effects of modern society on the global environment are becoming increasingly evident in the 21st century. Many of the environmental contaminants stem from society's reliance on hydrocarbon fuels. As traditional stocks of fossil fuels dwindle, new sources that require substantial processing are becoming more important. An archetypical example of this is the extraction of bitumen from oil sands deposits. Oil sands are naturally occurring mixtures of sand or clay, water, fine silts, and bitumen. Oil sands extraction processes at mines consume large volumes of water (*ca.* 3 barrels of fresh water for every 1 barrel of oil – Allen 2008, Canadian Association of Petroleum Producers 2012). Following bitumen extraction a tailings slurry is produced that consists of oil sands process-affected water (OSPW), sand, silt, clay particles, and trace quantities of unrecovered bitumen. This slurry is hydraulically transported to large area containment facilities (i.e., tailings ponds) that occupy approximately 130 km^2 with 200 million litres of mature fine tailings produced each day (Allen 2008). These vast storage facilities pose a potential risk to the environment, wildlife, and society (Misiti et al. 2013, Wang et al. 2013a).

Common constituents of OSPW include suspended solids, hydrocarbons, salts, chloride ions, ammonium ions, dissolved organic species (e.g., polycyclic aromatic hydrocarbons, benzothiophenes, dibenzothiophenes, and naphthenic acids), and trace heavy metals (Holowenko et al. 2002). Naphthenic acids (NAs; see Figure 1) are released from bitumen during caustic hot water digestion of oil sands ore, and are present at concentrations of approximately 40 to 120 mg/L (Headley and McMartin 2004, Holowenko et al. 2002, Kannel and Gan 2012). NAs are among the greatest environmental concerns associated with oil sands process-affected water (OSPW) because they are environmentally-persistent and acutely toxic toward aquatic life at the concentrations found in tailings pond water (Anderson et al. 2012, Melvin et al. 2013, Rogers et al. 2002, Sansom et al. 2013, Smits et al. 2012, Tollefsen et al. 2012, Wiseman et al. 2013).

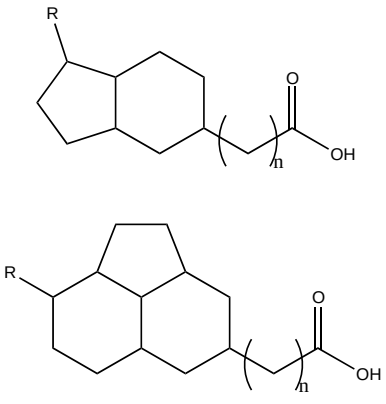

Figure 1. Representative naphthenic acid structures.

Responsible environmental stewardship of oil sands fossil fuel sources requires mitigation of the OSPW. Unfortunately no technologies currently exist that can effectively address this pressing challenge and the current state of political upheaval in other jurisdictions is increasing the demand for Canada's politically "safe" oil. Clearly, a solution to this problem is of *strategic* importance and novel benign-by-design technologies for remediating OSPW must be developed.

There are many candidate technologies that could be applied to the treatment of OSPW. Advanced oxidation processes (AOPs) are particularly useful for degrading biologically toxic or non-degradable materials such as aromatics, pesticides, petroleum constituents, and volatile organic compounds in wastewater. It has been reported by several researchers that exposing NAs to 254 nm ultraviolet (UV) radiation reduced their concentration and the overall aquatic toxicity (Gogate and Pandit 2004, Kannel and Gan 2012). Unfortunately, these approaches are very energy intensive and methods to increase both the efficacy and energy efficiency of AOPs must be explored. One avenue to achieve this is through the application of thoughtfully designed photocatalysts based on nanomaterials.

1.1 Engineered Nanoparticles for Contaminant Removal

Engineered nanoparticles (ENPs) continue to be the focus of extensive fundamental and practical scientific study partly because of their size and shape dependent optical, electronic, and chemical properties (Qu et al. 2013, Veinot 2006, Xu et al. 2013). The size dependency of these ENP characteristics is best exemplified by the optical response of semiconductor nanocrystals (NCs), which can be readily tuned throughout the electromagnetic spectrum by controlling particle size (Talapin et al. 2009) as shown in Figure 2.

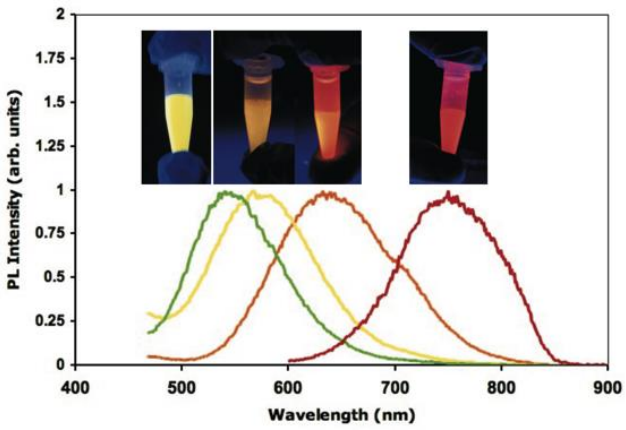

Figure 2. Photoluminescent response of hydride surface terminated Si engineered nanoparticles.
Particle size increases from left to right.

An often under-appreciated aspect of ENPs is their high surface area to volume ratio that makes it possible to tailor chemical compatibility (e.g., solubility), surface reactivity, and by extension

their interaction with their surroundings. Most importantly, the vast array of candidate materials and ENP properties offer scientists the unique opportunity to embrace the responsible "benign-by-design" approach noted above when preparing functional materials for specific applications; very simply, this revolutionary paradigm simply requires making the correct material choices.

In light of the exquisite tunability of ENPs and their properties, these materials are ideal candidates as active systems for remediation of anthropogenic environmental contaminants (Friedmann et al. 2010, Fujishima et al. 2008, Jaesang et al. 2011). Already, relatively simple "first generation" ENPs with limited tailoring of size and/or surface chemistry have provided important proof-of-concept in this regard. ENPs can also react with and/or induce reactions of molecules in solution. For example, photoexcitation of TiO_2 ENPs produces reactive oxygen species (ROS) such as ($O_2^{\bullet-}$), singlet oxygen ($^1O_2$), hydroxyl ($^{\bullet}OH$) and hydroperoxyl ($HO_2^{\bullet}$) radicals, and hydrogen peroxide (H_2O_2) (McMartin et al. 2004, Wang et al. 2013b). The generally accepted mechanism for this process is summarized in Figure 3(a).

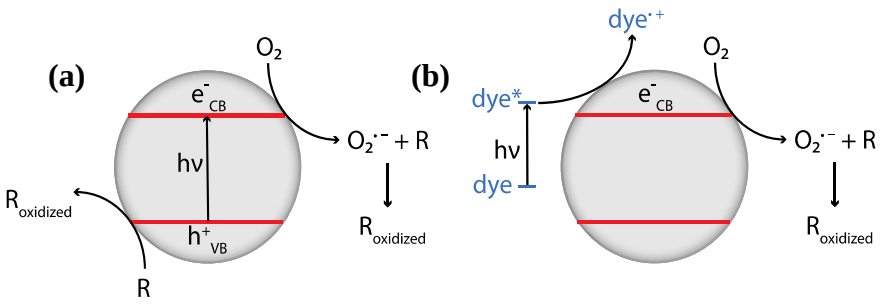

Figure 3. Two generally accepted mechanism for light induced degradation of organic compounds by semiconductor ENP.

Photoinduced reactions result from a band gap transition induced by exposure to light of an appropriate energy. For anatase TiO_2 (band gap *ca.* 3.2 eV), UV light possesses enough energy to promote an electron (e^-) across the band gap leaving a hole (h^+) in the valence band (VB). It has been proposed these "free" carriers are rapidly (i.e., on a picosecond time scale) trapped at various sites within the ENP core or at its surface. These excited-state ENPs can subsequently oxidize organic compounds via two pathways: (1) Direct oxidation at the ENP surface by reaction with the VB hole; and (2) Indirect oxidation by reactive oxygen species generated via reduction (i.e., reaction with a conduction band (CB) electron) of dissolved O_2. Reactive oxygen species formed at the engineered nanoparticle surface can diffuse away and the indirect oxidation reaction can proceed far (i.e., up to 1.1 μm in water) from the ENP (Chen et al. 2010). Similar reactions also occur with dye modified/sensitized semiconductor nanoparticles upon excitation with visible light (Figure 3(b)), suggesting the magnitude of the band gap energy is not a limiting factor in the production of ROS, rather the absolute energy of the surface trap states in which the electrons reside (Tachikawa and Majima 2009).

It has also been reported that the introduction of an insulating layer between the semiconductor core particle and a surface bonded dye moiety leads to improved activity in photochemical remediation (Chen et al. 2010).

These reported findings alone indicate it will be possible to treat OSPW effectively with ENPs and very likely lower the energy requirements of these processes and dramatically improve process efficiency through judicious choice of surface groups and controlling surface oxidation. Catalytic photoinduced oxidation of water-borne organic compounds (e.g., pharmaceuticals (An et al. 2010, Yang et al. 2010) and naphthenic acids (Kannel and Gan 2012)) has been demonstrated for surface modified and "naked" TiO_2 ENPs; unfortunately the quantum yield for the generation of hydroxyl radicals is relatively low (i.e., 0.04 to 0.05) (Sun and Bolton 1996). For this reason, it is necessary to rationally design future ENPs specifically for OSPW remediation.

Based on the accepted mechanism noted above, efficient trapping of electrons at ENP surfaces is essential, and it is desirable to locate target organic compounds (e.g., naphthenic acids) in close proximity to the ENP surface if reactivity is to be maximized.

To our knowledge, no efforts have been made to employ surface chemistry to locate target organic molecules close to the ENP surface. Clearly, semiconductor ENPs hold great promise in water treatment, including removing toxic organic compounds from OSPW and potentially solving the seemingly insurmountable problems associated with the toxic oil sands tailings ponds. Unfortunately, TiO_2 ENPs are environmentally persistent and have deleterious effects on biological systems (Marcone et al. 2012, Miller et al. 2012, Tong et al. 2013). Alternative semiconductor ENPs must be explored – silicon is environmentally and biologically benign and as a nanoparticle has a band gap *ca.* 2.5 eV making it an excellent candidate to replace TiO_2.

At the same time, synthesis of Si nanoparticles at a large scale is not commercially viable with the current methodologies (Veinot 2006). Thus, a cost effective and high yielding synthesis protocol needs to be developed for large scale applications (e.g., OSPW treatment) of Si nanoparticles.

2 SI NANOPARTICLE SYNTHESIS, FUNCTIONALIZATION AND CHARACTERIZATION

Si nanoparticles (Si NPs) of different size, crystallinity, and morphology were used to prepare candidate Si NP catalysts. The following particles were employed for the present study:

1. 3 nm Si NPs (3 nm)
2. 9 nm Si NPs (9 nm)
3. 100 nm Si NPs (100 nm)
4. >500 nm Si NPs (Si nanosponge)

General procedures for preparing Si NPs are summarized in Figure 4a. Small (i.e., diameter = 3 and 9 nm) Si NPs were obtained from thermal processing of hydrogen silsesquioxane (HSQ) (Hessel et al. 2006, Veinot 2006). Commercially available 100 nm Si particles were annealed in

a standard tube furnace at 1,100 °C in an Ar atmosphere, and Si nanosponge was synthesized by magnesiothermic reduction (Dasog et al. 2012).

All Si nanoparticle types (1 to 4) were etched using aqueous hydrofluoric acid (HF) to remove any silica and provide hydride surface groups that were further modified upon thermally induced hydrosilylation with dodecene (Hessel et al. 2006, 2007). The resulting alkyl surface terminated Si NPs were purified using standard procedures and are soluble in standard non-polar solvents (Figure 4(b)). Alkyl terminated Si NPs were rendered water soluble upon coating/intercalating with a known amphiphilic polymer (Figure 4(c)) (Lin et al. 2008).

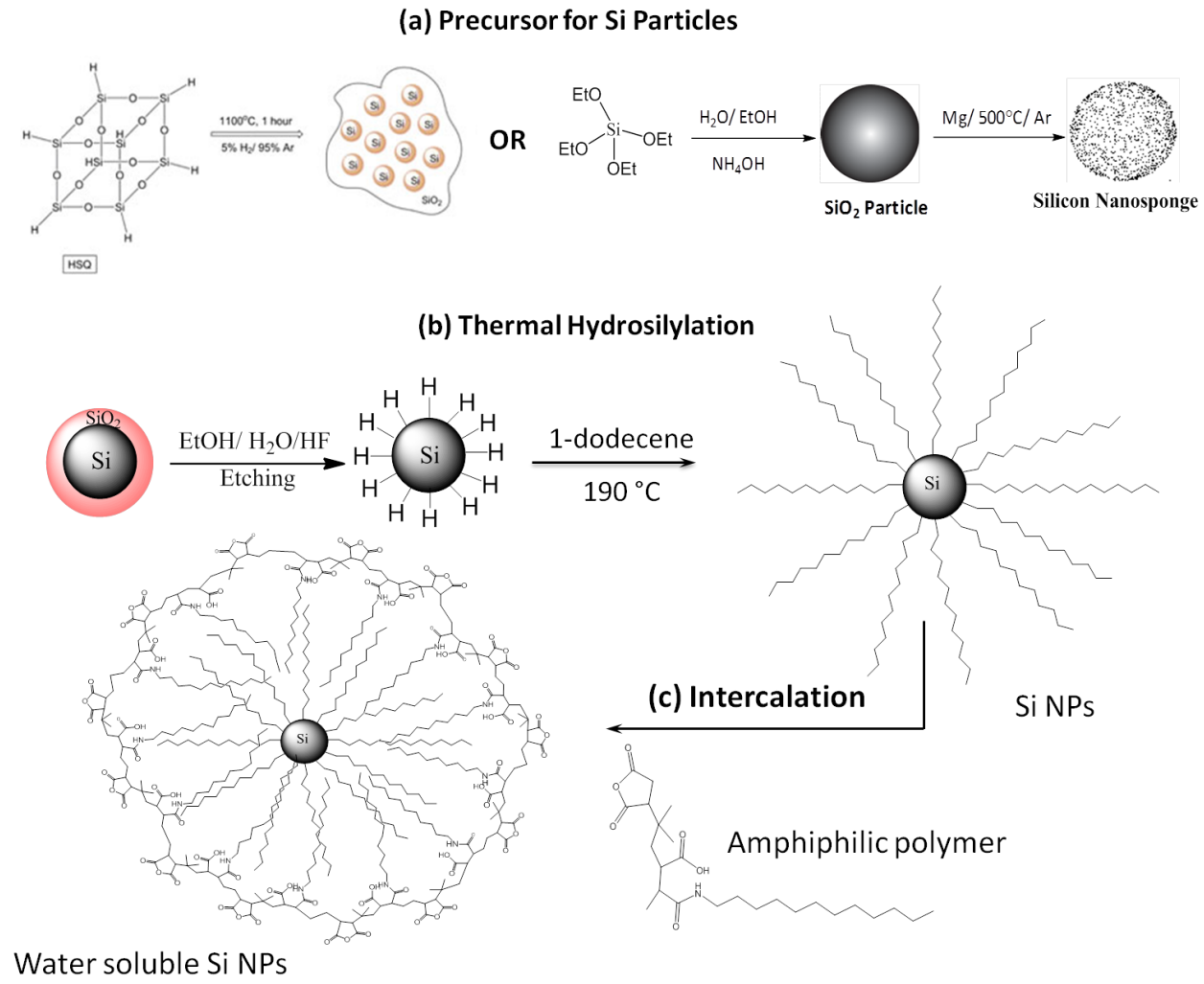

Figure 4. General scheme summarizing the preparation of water soluble Si nanoparticles. (a) Precursors for Si NPs (b) Thermal hydrosilylation and (c) Intercalation with amphiphilic polymer. (Note: EtOH = Ethanol, EtO = CH_3CH_2O, HF= Hydrofluoric acid).

All Si NPs were comprehensively characterized using Fourier-Transform Infrared Spectroscopy (FT-IR), scanning electron microscopy (SEM), transmission electron microscopy (TEM) and X-ray powder diffraction (XRD).

3 RESULTS AND DISCUSSION: SI NANOPARTICLE PREPARATION

All polymer-modified Si NPs absorb in the near-IR, UV and visible spectral regions (Figure 5).

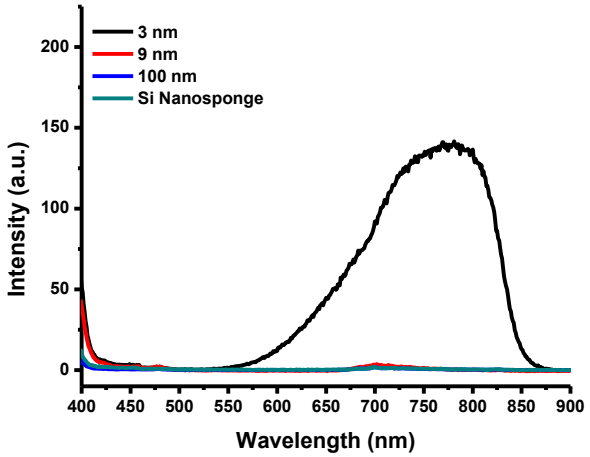

Figure 5. Photoluminescent emission spectra of water soluble Si nanoparticles upon excitation at 350 nm.

FT-IR analysis confirms all sizes of Si NPs modified via hydrosilylation with dodecene are alkyl surface terminated with negligible residual Si-H moieties and surface oxidation (Figure 6). Following dodecene functionalization, signature absorptions attributable to Si-H_x at 2,100 cm^{-1} are replaced by strong aliphatic C-H_x at 2,957, 2,925, and 2,853 cm^{-1} as well as C-CH_3 at 1,464 and 1,378 cm^{-1} (Henderson et al. 2009, Hessel et al. 2006).

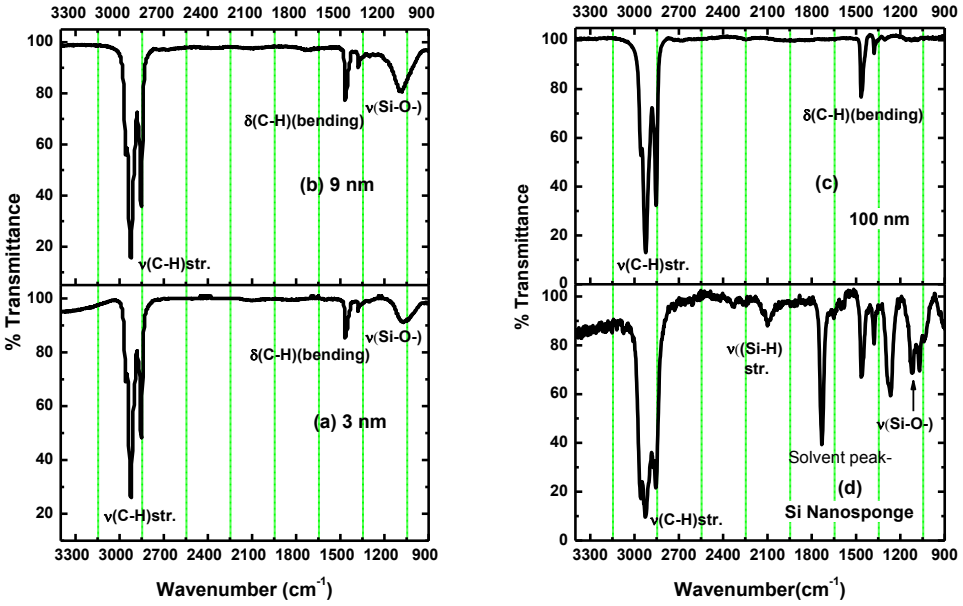

Figure 6. FT-IR spectra of alkyl functionalized Si NPs (a) 3nm (b) 9 nm (c) 100 nm and (d) Si nanosponge.

The FT-IR spectra of Si nanosponge shows evidence of trace oxide species and small quantities of Si-H_x (Figure 6(d)). In addition, we note the presence of characteristic C-H_x stretches and C-CH_3 deformations confirming these particles are also functionalized with dodecene.

X-ray powder diffraction (XRD) data for all investigated Si NPs show reflections at 28°, 48°, 56°, 69° and 77° corresponding to reflections from the (111), (220), (311), (400) and (331) crystallographic planes of diamond cubic Si, indicating the Si NP core was not compromised during functionalization (Hessel et al. 2007). Diffraction signals arising from d = 100 nm and >500 nm Si nanosponge (Figure 7) are intense and sharp, consistent with the size of the particles. The diffraction pattern obtained from d = 3 nm and 9 nm Si NPs show broad signals indicative of their smaller dimensions (Hessel et al. 2010).

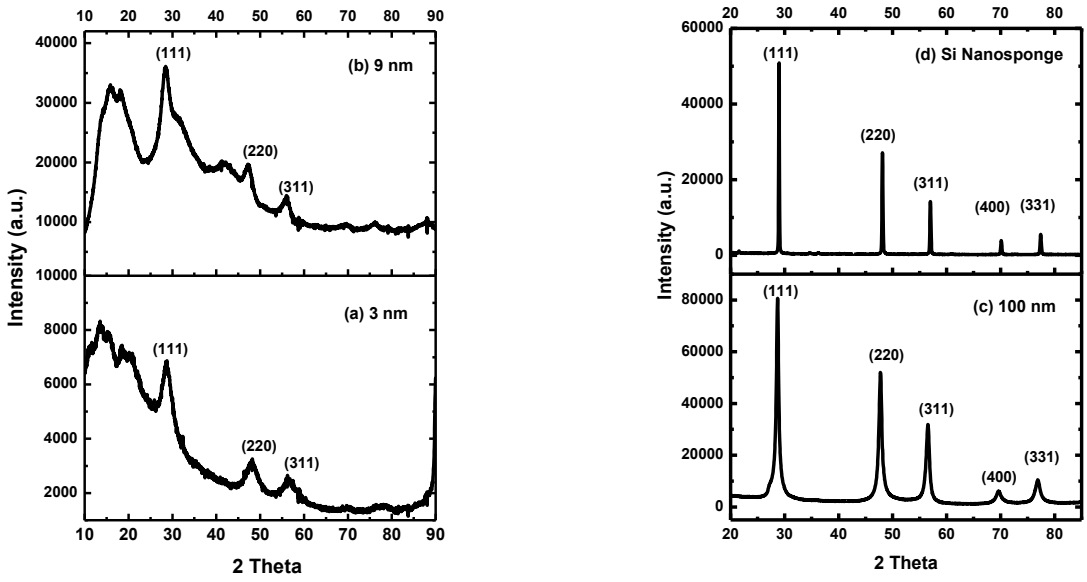

Figure 7. XRD patterns of Si nanoparticles.
(a) 3 nm (b) 9 nm (c) 100 nm NPs and (d) Si nanosponge.

Transmission electron microscopy (TEM) and scanning electron microscopy (SEM) were employed to evaluate the morphology and size of the Si NPs. As expected, the dimensions of pseudospherical Si NPs obtained from thermal processing of hydrogen silsesquioxane (HSQ) were dependent upon thermal processing temperature and samples with average diameters of 3 and 9 nm were obtained (See Figure 8a,b) (Hessel et al. 2006, 2007).

Si NPs obtained from HF etching of a commercial Si powder (Strem Chemicals Inc.) was also pseudospherical with average diameters of *ca.* 100 nm (Figure 8c).

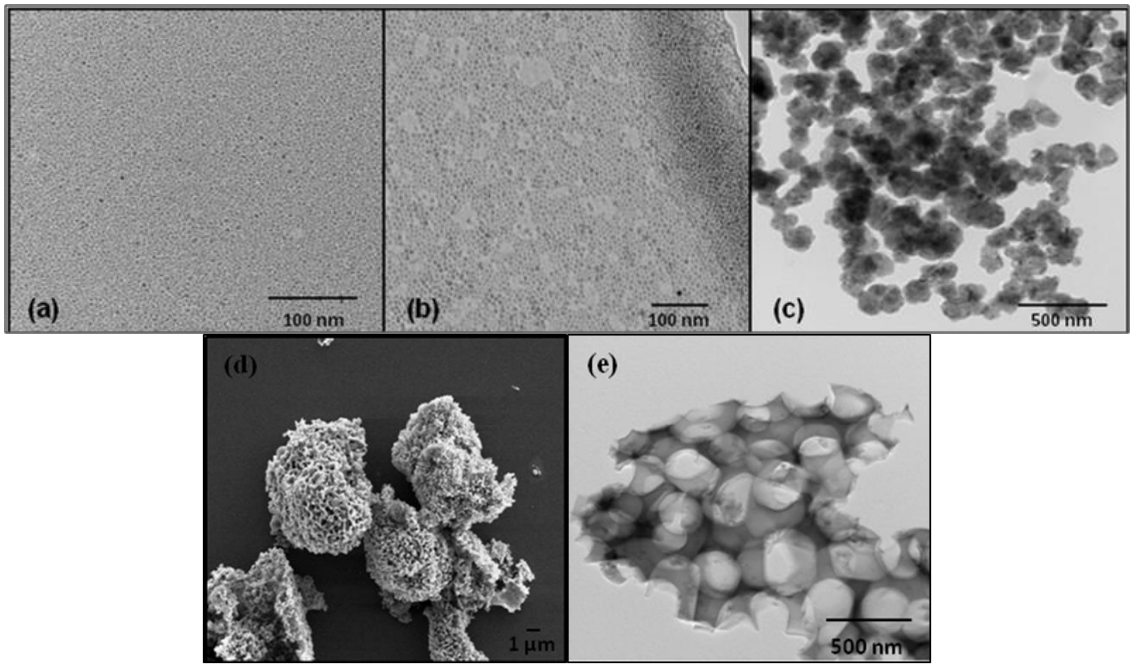

Figure 8. TEM images of Si nanoparticles.
(a) 3 nm (b) 9 nm (c) 100 nm (d) SEM image of Si nanosponge and (e) TEM image of Si nanosponge.

An alternative nanoscale morphology (i.e., nanosponge) of Si was obtained from Mg reductions of sol-gel derived SiO_2 templates. SEM analysis shows comparatively larger particles (d = hundreds of nm) possessing randomly distributed pseudospherical pores (i.e., d ~ 25 nm) (Figure 8d and e).

4 REMEDIATION STUDIES ON CONTAMINANTS

To evaluate the activity of the Si nanomaterials for light induced remediation of organic contaminants in water, a standard model contaminant (i.e., methanol) was employed. The intent of this study was to establish appropriate treatment conditions that lead to production of reactive oxygen species (ROS) and optimize reactivity. Advanced oxidation process (AOP) based contaminant removal was carried out using the Si NPs.

4.1 Experimental Design

A quasi-collimated beam UV apparatus (Calgon Carbon Corporation, Pittsburgh, USA) equipped with a 1 kW medium pressure lamp (HNG, Hanau, Germany) was used to generate a quasi-parallel beam of UV light as shown in Figure 9.

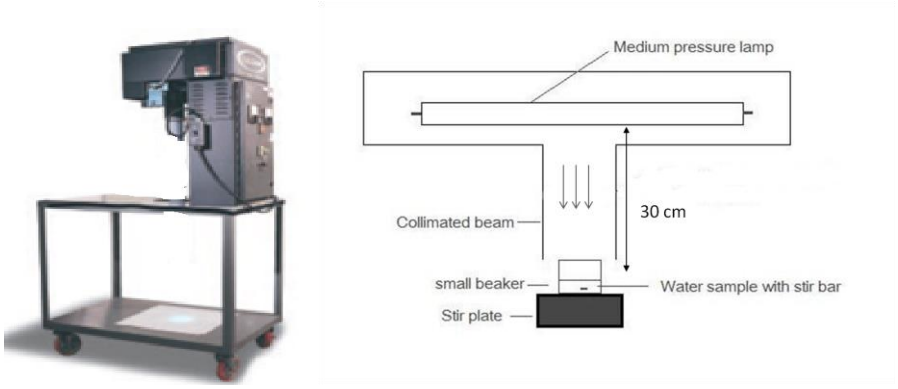

Figure 9. (a) A quasi-collimated beam UV apparatus and (b) a schematic of remediation experiment in a quasi-collimated beam.

The incident irradiance at the water surface for each sample was quantified using a radiometer (International Light, Model IL1400, Massachusetts, USA) and UV detector (International Light, Model SEL240, Massachusetts, USA). The relative sensitivity of the detector was determined to be between 200 and 400 nm by the supplier. The irradiance was measured by placing the UV detector at the center of the collimated beam and adjusting the calibration marker on the detector to the height of the solution surface.

A known volume (i.e., 10 mL) of a solution containing predetermined concentrations of Si NPs (i.e., 50 mg/L and 100 mg/L) and methanol (Table 1) was placed in a 20 mL beaker with a 3.0 cm internal diameter and thermostated at 25 ± 2°C. The solution was then mechanically stirred using a magnetic stir bar (3 × 10 mm) to ensure homogenous and complete mixing during the reaction. For all evaluations the distance between the lamp solution surfaces was maintained at 30 cm. Solutions were exposed to the UV for 10 and 30 minutes. A schematic of the remediation experiment set up used is presented in Figure 9(b).

Table 1. Methanol concentrations employed during model remediation studies.

Methanol concentration	**mg/L**	2.5	5	10	20	30	40	50
	mM	0.078	0.0156	0.312	0.624	0.936	1.248	1.561

4.2 Sample Analysis

Methanol oxidizes to formaldehyde and the amount of formaldehyde can be determined by means of Nash colorimetric test (Chan et al. 2012, Nash 1953). The Nash reagent was prepared by mixing 2 M ammonium acetate, 0.05 M acetic acid and 0.02 M acetylacetone in 1L of deionized water. Five millilitres of freshly prepared Nash reagent was added to five millilitres of

"remediated" samples and the mixture was incubated at 40 °C for 60 minutes. The amount of diacetyl-dihydro-lutidine (DDL) produced was determined by evaluating the absorption spectrum of the solution at 412 nm and comparing with the standard curve data shown in Figure 10 (a).

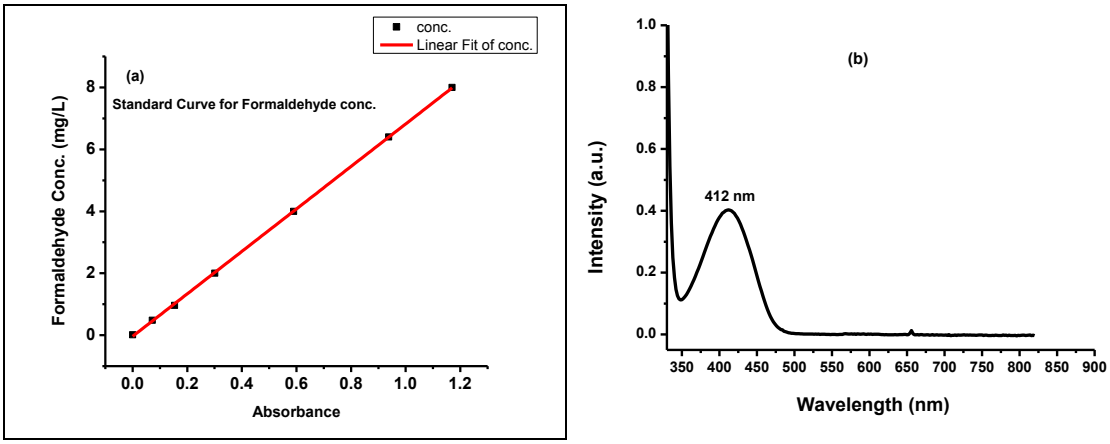

Figure 10. (a) Standardization curve to determine the formaldehyde concentration and (b) a representative UV-Vis plot of Si NPs upon incubation with Nash reagent.

4.3 Determination of Quantum Yield and Hydroxyl Radical Yield Factor

The quantum yield for the generation of ·OH radicals plays a very important role in determining the efficiency of the photodegradation of pollutants. Similarly, the rate constant determines the rate of photoreaction at a particular UV dose.

The quantum yield (QY) of the Si NP-induced formation of formaldehyde was determined using the following standard procedure as reported by (Bolton and Stefan 2002, Jin et al. 2011, Sun and Bolton 1996):

$$\boldsymbol{\Phi} = \frac{\textit{moles of product formed or reactant removed}}{\textit{einsteins of photons absorbed}} \quad \textbf{(1)}$$

$$K_1' = \ln\left(\frac{C_0}{C_F}\right)/F \quad \textbf{(2)}$$

$$F = E_{op}' U_\lambda (WF)(DF)(PF)(RF)t = E_{op}'(avg) U_\lambda t \quad \textbf{(3)}$$

$$\Phi_c = 10 K_1' U_\lambda / [\ln(10)\, \varepsilon_C] \quad \textbf{(4)}$$

Where,

Φ = quantum yield

K_1' = fluence-based first-order 'rate constant' ($m^2\ J^{-1}$)

ε_C = molar absorption coefficient ($M^{-1}\ cm^{-1}$) for methanol

C_0 and C_F = the initial and final concentrations of methanol under photolysis

F = fluence ($J\ m^{-2}$)

E'_{op} = incident photon fluence rate (einstein $s^{-1}\ m^{-2}$)

E'_{op} (avg) = average photon fluence rate in the solution

U_λ = molar photon energy (J $einstein^{-1}$)

The water factor (WF), divergence factor (DF), Petri factor (PF), and reflection factor (RF) were calculated using the procedure previously reported (Bolton and Linden 2003).

The formation of hydroxyl radicals (·OH) is directly related to the UV photolysis process. The concentration of the ·OH radicals generated may be quantified by evaluating the formation of formaldehyde in the presence of excess methanol (Sun and Bolton 1996). Formaldehyde concentration quantification was achieved using the Nash method (see above). Yield factor (η) can be quantified as follows:

$$\eta = \frac{\Delta[\cdot OH]}{\Delta[HCOH]} \qquad \textbf{(5)}$$

where the hydroxyl radical concentration [·OH] is determined from the concentration of formaldehyde produced during photolysis.

5 RESULTS AND DISCUSSION: CONTAMINANT REMEDIATION

Various parameters affecting the quantum yield (QY) and fluence-based first-order rate constant (K_1') were methodically investigated including NP size and morphology, NP concentration, methanol concentration, and exposure time.

5.1 Quantum Yields (QYs) and K_1' of Si Nanoparticles

Two mass concentrations (100 and 50 mg/L) of functionalized 3 nm Si NPs and exposure times (10 min and 30 min) were employed for photocatalytic oxidation of methanol to formaldehyde. The QYs and fluence-based rate constants K_1' were determined.

The analysis shows 100 mg/L solutions of 3 nm Si NPs and exposure times of 10 minutes consistently showed significantly higher QYs and K_1' for all concentrations of methanol tested (Figure 11). Solutions of 3 nm Si NPs of 50 mg/L and 100 mg/L concentrations exhibited near identical QYs and K_1' when exposed for 10 and 30 minutes, respectively, while 50 mg/L solutions of 3 nm Si NPs exposed for 30 minutes showed the lowest performance metrics for all concentrations of methanol tested.

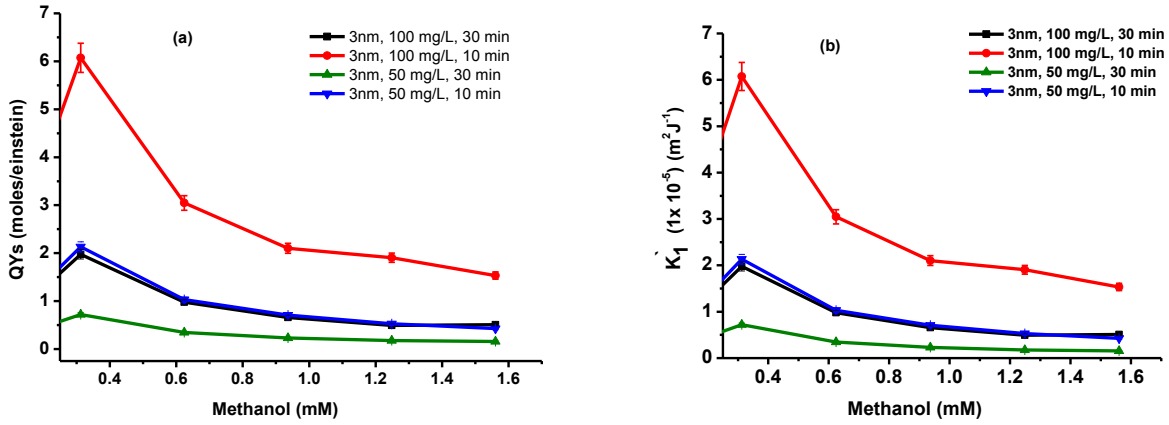

Figure 11. Effect of Si nanoparticle concentration on (a) QY and (b) K_1'.

Based upon these results it was determined that 100 mg/L was the optimum Si NP concentration and was used for all subsequent experiments.

The influence of Si NP size was evaluated for 100 mg/L NP solutions by evaluating methanol photolysis QYs. Data are summarized in Figure 12. To our surprise, the 100 nm Si NPs showed highest QYs regardless of exposure time. However, Si NPs exposed to UV irradiation for 10 minutes showed significantly higher QYs (i.e., 2 to 3 times) when compared to the 30 minute exposures for all sizes.

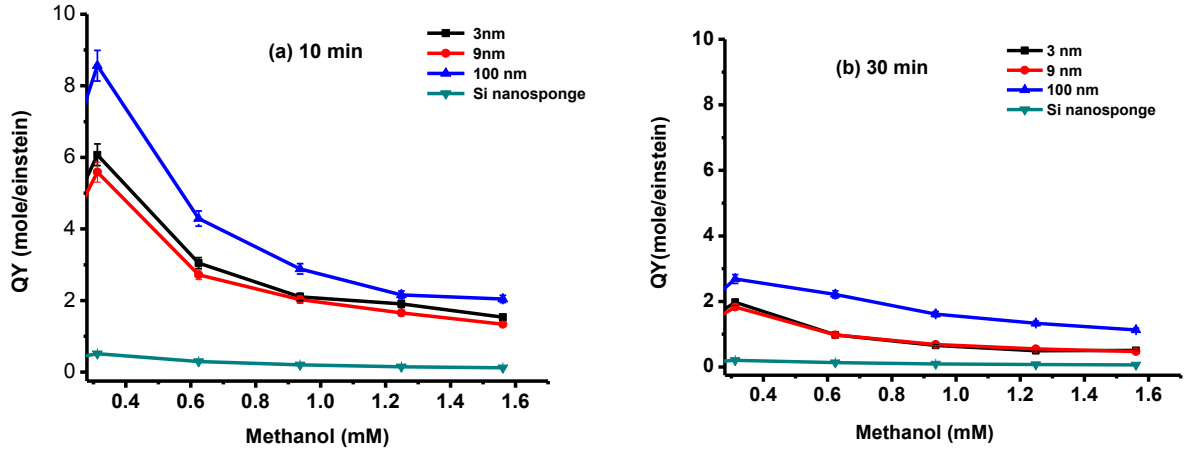

Figure 12. Effect of size on the QYs of Si NPs when exposed for (a) 10 minutes (b) 30 minutes to UV light.

In addition to possible size effects, several additional factors can contribute to the photocatalytic activity of Si NPs, chief among them are photoluminescent (PL) response, band gap, surface

structure and surface chemistry. It is reasonable that photoluminescent Si nanocrystals (i.e., d = 3 nm and 9 nm) will exhibit lower remediation efficiency metrics because some energy (at least 5% based upon established PL QYs) is lost through the radiative recombination processes. However, another important factor is the presence of surface structure. It is expected that large (d = 100 nm) Si NPs have a more complex surface structure leading to more reactive sites. In addition, the narrower band gap of the larger particles (i.e., 1.1 eV) will facilitate absorption of more incident light energy. Photoexcited Si NPs can, in turn oxidize organic compounds *via* direct oxidation at the nanocrystal surface by valence band hole, or indirect oxidation by reactive oxygen species (ROS) through reaction with a defect state electron or valence band electron (Panayotov et al. 2012, 2013, Qu and Duan 2010, 2013, Wang et al. 2013b).

Finally, coating the surfaces of Si nanoparticles with the amphiphilic polymer provides medium compatibility and partitioning of pollutants close to the reactive surface. The partitioning of the pollutant was confirmed by adding a known concentration of Rhodamine 6G dye (20 mg/L) to 10 mL of Si NP solutions (100 mg/L). The solution was incubated for 30 min and then centrifuged. Most of the dye partitioned with the Si NPs and precipitated out (Figure 13) confirming that pollutants are getting partitioned near the NP surfaces.

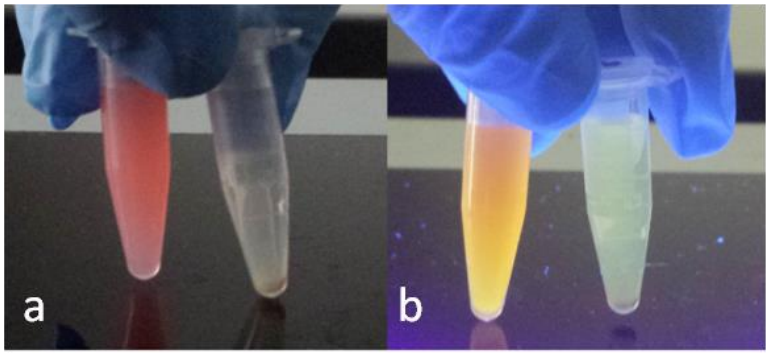

Figure 13**.** Partitioning of Rhodamine 6G with 100 nm Si NPs.
(a) Under regular light and (b) under UV illumination at 365 nm.
Samples on the left in (a) and (b) are before centrifugation while samples on the right are after centrifugation. (Note: the color is arising from the dye not from the Si NPs).
Rhodamine is used as a surrogate for how organic contaminants would be affected.

Our results indicate longer UV exposure does not necessarily translate into higher QYs. We attribute this to the majority of the methanol being photocatalytically converted to formaldehyde during the initial 10 minutes of exposure. In this context, the energy from photons absorbed after 10 minutes of reaction is largely dissipated.

As expected, similar trends to those noted for QY evaluation were seen in the evaluation/evolution of the pseudo first order constant K_1' for all NP systems (Figure 14).

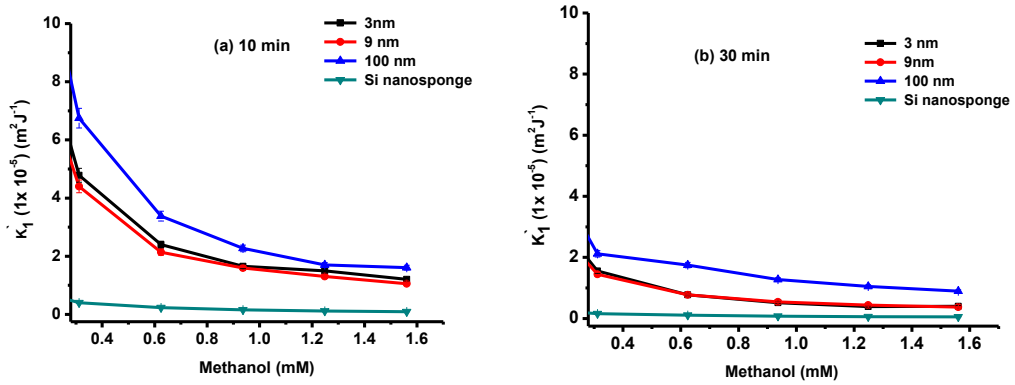

Figure 14. Effect of size on K_1' of Si NPs when exposed for (a) 10 minutes (b) 30 minutes to UV light.

5.2 Yield Factors (η) for the Generation of ·OH Radicals

To investigate the ·OH radical production and photolysis yield factor, the production of formaldehyde was again evaluated for the samples that contained methanol. The ·OH radical formation can be determined by the amount of formaldehyde produced (equation 5). The relationship between formaldehyde production and methanol concentration is shown in Figure 15. Yield factors are provided as numeric annotations for 0.94 mM (30 mg/L) of methanol and indicated exposure times.

We note that in all cases the formaldehyde production increased with methanol concentration increases; however, with time this process slows down once methanol becomes the dominant reactant with the Si NPs. These results indicate that at high concentrations of methanol, production of formaldehyde becomes pseudo independent of methanol concentration.

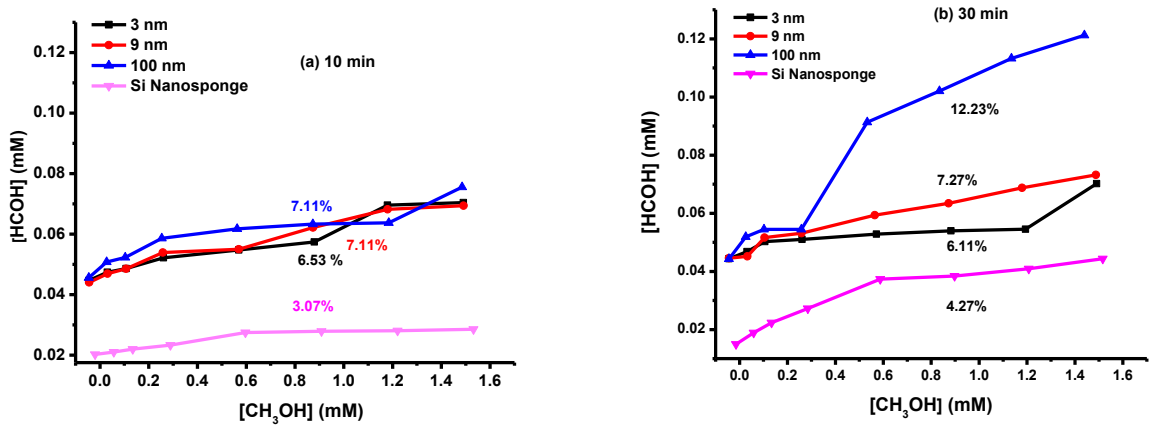

Figure 15. Formaldehyde production as function of methanol concentration (mM) and yield factors (η) of ·OH radical production in the photolysis when UV exposure time was (a) 10 min and (b) 30 min.

The yield factors for the samples were calculated by evaluating the ratio of ·OH produced and methanol decomposed during the photolysis. As is evident from Figure 15, yield factors increased with an increase in methanol concentration.

The increase in yield factors slowed for all sizes of Si NPs when methanol concentrations were increased above 0.4 mM during photolysis for 10 minutes. 100 nm Si NPs showed comparatively higher yield factors versus their 3 and 9 nm counterparts. In contrast, when exposed for 30 minutes, 100 nm Si NPs showed consistently higher yield factors (>10) for methanol concentrations higher than 0.4 mM while the yield factors for 3 and 9 nm Si NPs were comparable to those observed for 10 minutes of photolysis.

Of important note, the yield factors determined here are two to three times higher than equivalent values obtained for various TiO_2 nanoparticles systems (e.g., bare particles or modified TiO_2 nanocomposites or metal-semiconductor) (Wang et al. 2000, Wang et al. 2002, Wang et al. 2013b).

6 CONCLUSIONS AND RECOMMENDATIONS

6.1 Conclusions

Si NPs of different sizes were synthesized by means of established procedures, functionalized and later employed for advanced oxidation processes by means of photolysis. A cost effective and high yielding magnesiothermic reduction protocol for the synthesis of Si NPs has been developed. The new Mg-reduction method paves the way for large scale synthesis (i.e., kilograms) of Si nanoparticles of tailored size and shape, which in turn opens up possibilities of industrial scale Si NP applications.

UV advanced oxidation processes (AOPs) are often used as an effective mitigation protocol to address the impact of organic pollutants. The combination of UV photolysis and hydroxyl (OH) radical reactions ensures the removal of a wide range of compounds. In this study, the UV/Si NPs system was used for the oxidation of a model contaminant, methanol. It was determined that UV exposure of 10 minutes in the presence of Si nanoparticles is suitable to degrade the model contaminant with appreciably higher quantum yields and reaction rates than standard TiO_2 systems. The yield factors (η) obtained also exceeded those reported in the literature for TiO_2 based systems. Contrary to our original hypothesis that the NP band gap would dictate remediation efficiency, larger Si NPs (100 nm) exhibited consistently higher QYs and yield factors compared to their smaller Si NP counterparts. This observation is postulated to result from a manifestation of energy losses incurred during photoluminescence processes. We also suggest here that the presence of surface suboxides and surface structure may contribute to the increased efficacy of the 100 nm diameter particles in photocatalytic applications. In this context, we conclude that the intrinsic nanoparticle properties (e.g., crystallinity, defects, surface structure, suboxides, among others) play crucial roles in Si nanoparticle photocatalysis that can override nanoparticle size effects.

The quantum yields obtained for Si NPs are unprecedented and provide comprehensive evidence that Si nanoparticles are highly suitable for wastewater treatment. Adding to their appeal, Si nanoparticles are bio-inert, possess highly tunable surface chemistry, and have a tunable band-gap. These properties alone make Si nanoparticles a material of choice for environmental remediation and an ideal replacement for TiO_2 based systems. The use of Si nanoparticles helps to overcome several disadvantages of TiO_2-based photocatalysts; for example, TiO_2 can only absorb 5% of solar spectrum energy due to its wide band gap and faster recombination rates making it an inefficient solar-based photocatalyst. The band gap of large Si nanoparticles allows absorption of more than 50% of the solar spectrum (Shockley and Queisser 1961) making passive solar induced remediation of organic pollutants a viable option.

This study is the first detailed investigation of the photocatalytic efficiency of Si nanoparticles for the oxidation of organic contaminants. The results are very promising and Si NPs have emerged as potential candidate for applications in OSPW treatment.

6.2 Recommendations

The following recommendations are put forth based on the current results and understanding of photocatalytic activity of Si nanoparticles.

1. It is important that the scope of current studies be expanded to more complex molecules such as cyclohexanoic acid (CHA) or acids with multiple aromatic rings that serve as more accurate analogues of the naphthenic acids present in OSPW. The optimal concentrations of Si NPs and exposure times obtained here for methanol oxidation serve as guides in choosing the appropriate conditions for more advanced treatment. The degradation by-products of CHA and related compounds should be thoroughly investigated using mass spectrometry (LC-MS) techniques.

2. The pH of OSPW is approximately 8 to 8.4. In this context, the remediation of CHA and other complex models should be tested at appropriate OSPW pH conditions. Similarly, the presence of various salts or ions (e.g., $Cl^-$and/or CO_3^{2-}) have been implicated in the scavenging of OH radicals. It is paramount that detailed studies are carried out to evaluate the photocatalytic efficiency of Si NPs in the presence of these scavengers and other environmentally relevant chemicals.
3. Authentic OSPW samples obtained from different sources should also be tested using UV/Si nanoparticle AOP processes. The degradation by-products are expected to be very complex mixtures owing to the complex nature of organics present in OSPW. However, these by-products can be identified and quantified by means of mass spectrometry.
4. It is also recommended that suitable technology be developed for homogenous additions of Si nanoparticles into flowthrough reactors and that scalable hydraulically efficient reactors with suitable nanomaterial injection systems are designed. The design and fabrication of laboratory-scale reactors will allow for effective evaluation of the efficacy of nanoparticles in OSPW degradation. A number of important parameters must be evaluated: (i) the intensity/energy of light requirements for the degradation of naphthenic acids by nanoparticles, (ii) reaction kinetics using various co-reactants, (iii) effectiveness or QYs of Si nanoparticles for naphthenic acid degradation, and (iv) evaluation of reaction by-products.

An important component of a reactor system of this type would immobilize optimized Si nanoparticles on porous ceramic membranes and provide a continuous system for contaminant degradation in flow through reactors.

7 REFERENCES

Allen, E.W., 2008. Process water treatment in Canada's oil sands industry: I. Target pollutants and treatment objectives. Journal of Environmental Engineering and Science 7(2) 123-138.

An, T., H. Yang, G. Li, W. Song, W.J. Cooper and X. Nie, 2010. Kinetics and mechanism of advanced oxidation processes (AOPs) in degradation of ciprofloxacin in water. Applied Catalysis B: Environmental 94(3-4): 288-294.

Anderson, J., S.B. Wiseman, A. Moustafa, M. Gamal El-Din, K. Liber and J.P. Giesy, 2012. Effects of exposure to oil sands process-affected water from experimental reclamation ponds on *Chironomus dilutus*. Water Research 46(6): 1662-1672.

Bolton, J. and K. Linden, 2003. Standardization of methods for fluence (UV dose) determination in bench-scale UV experiments. Journal of Environmental Engineering 129(3): 209-215.

Bolton, J. and M. Stefan, 2002. Fundamental photochemical approach to the concepts of fluence (UV dose) and electrical energy efficiency in photochemical degradation reactions. Research on Chemical Intermediates 28(7-9): 857-870.

Canadian Association of Petroleum Producers, 2012. Water use in Canada's oil sands. Canadian Association of Petroleum Producers, Calgary, Alberta. 8 pp.

Chan, P.Y., M. Gamal El-Din and J.R. Bolton, 2012. A solar-driven UV/chlorine advanced oxidation process. Water Research 46(17): 5672-5682.

Chen, C., W. Ma and J. Zhao, 2010. Semiconductor-mediated photodegradation of pollutants under visible-light irradiation. Chemical Society Reviews 39(11): 4206-4219.

Dasog, M., Z. Yang and J.G.C. Veinot, 2012. Size-controlled solid state synthesis of luminescent silicon nanocrystals using Stober silica particles. CrystEngComm 14(22): 7576-7578.

Friedmann, D., C. Mendive and D. Bahnemann, 2010. TiO_2 for water treatment: Parameters affecting the kinetics and mechanisms of photocatalysis. Applied Catalysis B: Environmental 99(3-4): 398-406.

Fujishima, A., X. Zhang and D.A. Tryk, 2008. TiO2 photocatalysis and related surface phenomena. Surface Science Reports 63(12): 515-582.

Gogate, P.R. and A.B. Pandit, 2004. A review of imperative technologies for wastewater treatment I: Oxidation technologies at ambient conditions. Advances in Environmental Research 8(3-4): 501-551.

Headley, J.V. and D.W. McMartin, 2004. A review of the occurrence and fate of naphthenic acids in aquatic environments. Journal of Environmental Science and Health – Part A Toxic/Hazardous Substances and Environmental Engineering 39(8): 1989-2010.

Henderson, E.J., J.A. Kelly and J.G.C. Veinot, 2009. Influence of HSiO1.5 sol-gel polymer structure and composition on the size and luminescent properties of silicon nanocrystals. Chemistry of Materials 21(22): 5426-5434.

Hessel, C.M., E.J. Henderson and J.G.C. Veinot, 2006. Hydrogen silsesquioxane: A molecular precursor for nanocrystalline Si-SiO_2 composites and freestanding hydride-surface-terminated silicon nanoparticles. Chemistry of Materials 18(26): 6139-6146.

Hessel, C.M., E.J. Henderson and J.G.C. Veinot, 2007. An investigation of the formation and growth of oxide-embedded silicon nanocrystals in hydrogen silsesquioxane-derived nanocomposites. Journal of Physical Chemistry C 111(19): 6956-6961.

Hessel, C.M., M.R. Rasch, J.L. Hueso, B.W. Goodfellow, V.A. Akhavan, P. Puvanakrishnan, J.W. Tunnel and B.A. Korgel, 2010. Alkyl passivation and amphiphilic polymer coating of silicon nanocrystals for diagnostic imaging. Small 6(18): 2026-2034.

Holowenko, F.M., M.D. MacKinnon and P.M. Fedorak, 2002. Characterization of naphthenic acids in oil sands wastewaters by gas chromatography-mass spectrometry. Water Research 36(11): 2843-2855.

Jaesang, L., K. Jungwon and C. Wonyong, 2011. Aquatic redox chemistry. American Chemical Society, Washington, D.C. pp. 199-222.

Jin, J., M.G. El-Din and J.R. Bolton, 2011. Assessment of the UV/chlorine process as an advanced oxidation process. Water Research 45(4): 1890-1896.

Kannel, P.R. and T.Y. Gan, 2012. Naphthenic acids degradation and toxicity mitigation in tailings wastewater systems and aquatic environments: A review. Journal of Environmental Science and Health – Part A Toxic/Hazardous Substances and Environmental Engineering 47(1): 1-21.

Lin, C.A.J., R.A. Sperling, J.K. Li, T.Y. Yang, P.Y. Li, M. Zanella, W.H. Chang and W.J. Parak, 2008. Design of an amphiphilic polymer for nanoparticle coating and functionalization. Small 4(3): 334-341.

Marcone, G.P.S., A.C. Oliveira, G. Almeida, G.A. Umbuzeiro and W.F. Jardim, 2012. Ecotoxicity of TiO_2 to Daphnia similis under irradiation. Journal of Hazardous Materials 211-212: 436-442.

McMartin, D.W., J.V. Headley, D.A. Friesen, K.M. Peru and J.A. Gillies, 2004. Photolysis of naphthenic acids in natural surface water. Journal of Environmental Science and Health, Part A 39(6): 1361-1383.

Melvin, S.D., C.M. Lanctôt, P.M. Craig, T.W. Moon, K.M. Peru, J.V. Headley and V.L. Trudeau, 2013. Effects of naphthenic acid exposure on development and liver metabolic processes in anuran tadpoles. Environmental Pollution 177: 22-27.

Miller, R.J., S. Bennett, A.A. Keller, S. Pease and H.S. Lenihan, 2012. TiO_2 nanoparticles are phototoxic to marine phytoplankton. PLoS One 7(1), e30321.

Misiti, T., U. Tezel and S.G. Pavlostathis, 2013. Fate and effect of naphthenic acids on oil refinery activated sludge wastewater treatment systems. Water Research 47(1): 449-460.

Nash, T., 1953. The colorimetric estimation of formaldehyde by means of the Hantzsch reaction. The Biochemical Journal 55(3): 416-421.

Panayotov, D.A., S.P. Burrows and J.R. Morris, 2012. Photooxidation mechanism of methanol on rutile TiO_2 nanoparticles. Journal of Physical Chemistry C 116(11): 6623-6635.

Panayotov, D.A., P.A. DeSario, J.J. Pietron, T.H. Brintlinger, L.C. Szymczak, D.R. Rolison and J.R. Morris, 2013. Ultraviolet and visible photochemistry of methanol at 3D mesoporous networks: TiO_2 and Au-TiO_2. Journal of Physical Chemistry C 117(29): 15035-15049.

Qu, X., P.J.J. Alvarez and Q. Li, 2013. Applications of nanotechnology in water and wastewater treatment. Water Research 47(12): 3931-3946.

Qu, Y. and X. Duan, 2010. Highly efficient photocatalysts from nanoscale metal/semiconductor/metal heterojunctions. ECS Transactions 33(9): 23-38.

Qu, Y. and X. Duan, 2013. Progress, challenge and perspective of heterogeneous photocatalysts. Chemical Society Reviews 42(7): 2568-2580.

Rogers, V.V., M. Wickstrom, K. Liber and M.D. MacKinnon, 2002. Acute and subchronic mammalian toxicity of naphthenic acids from oil sands tailings. Toxicological Sciences 66(2): 347-355.

Sansom, B., N.T.K. Vo, R. Kavanagh, R. Hanner, M. MacKinnon, D.G. Dixon and L.E.J. Lee, 2013. Rapid assessment of the toxicity of oil sands process-affected waters using fish cell lines. In Vitro Cellular and Developmental Biology - Animal 49(1): 52-65.

Shockley, W. and H.J. Queisser, 1961. Detailed balance limit of efficiency of p-n junction solar cells. Journal of Applied Physics 32(3): 510-519.

Smits, J.E.G., B.D. Hersikorn, R.F. Young and P.M. Fedorak, 2012. Physiological effects and tissue residues from exposure of leopard frogs to commercial naphthenic acids. Science of The Total Environment 437: 36-41.

Sun, L. and J.R. Bolton, 1996. Determination of the quantum yield for the photochemical generation of hydroxyl radicals in TiO_2 suspensions. The Journal of Physical Chemistry 100(10): 4127-4134.

Tachikawa, T. and T. Majima, 2009. Single-molecule fluorescence imaging of TiO_2 photocatalytic reactions. Langmuir 25(14): 7791-7802.

Talapin, D.V., J-S. Lee, M.V. Kovalenko and E.V. Shevchenko, 2009. Prospects of colloidal nanocrystals for electronic and optoelectronic applications. Chemical Reviews 110(1): 389-458.

Tollefsen, K.E., K. Petersen and S.J. Rowland, 2012. Toxicity of synthetic naphthenic acids and mixtures of these to fish liver cells. Environmental Science and Technology 46(9): 5143-5150.

Tong, T., C.T.T. Binh, J.J. Kelly, J-F. Gaillard and K.A. Gray, 2013. Cytotoxicity of commercial nano-TiO_2 to *Escherichia coli* assessed by high-throughput screening: Effects of environmental factors. Water Research 47(7): 2352-2362.

Veinot, J.G.C., 2006. Synthesis, surface functionalization, and properties of freestanding silicon nanocrystals. Chemical Communications 40: 4160-4168.

Wang, B., Y. Wan, Y. Gao, M. Yang and J. Hu, 2013a. Determination and characterization of oxy-naphthenic acids in oilfield wastewater. Environmental Science and Technology 47(16): 9545-9554.

Wang, C., D.W. Bahnemann and J.K. Dohrmann, 2000. A novel preparation of iron-doped TiO2 nanoparticles with enhanced photocatalytic activity. Chemical Communications 16: 1539-1540.

Wang, C., H. Liu and Y. Qu, 2013b. TiO_2-based photocatalytic process for purification of polluted water: bridging fundamentals to applications. Journal of Nanomaterials 2013: 319637 (14 pp.).

Wang, C., J. Rabani, D.W. Bahnemann and J.K. Dohrmann, 2002. Photonic efficiency and quantum yield of formaldehyde formation from methanol in the presence of various TiO_2 photocatalysts. Journal of Photochemistry and Photobiology A: Chemistry 148(1-3): 169-176.

Wiseman, S.B., J.C. Anderson, K. Liber and J.P. Giesy, 2013. Endocrine disruption and oxidative stress in larvae of *Chironomus dilutus* following short-term exposure to fresh or aged oil sands process-affected water. Aquatic Toxicology 142-143: 414-421.

Xu, L., W. Ma, L. Wang, C. Xu, H. Kuang and N.A. Kotov, 2013. Nanoparticle assemblies: dimensional transformation of nanomaterials and scalability. Chemical Society Reviews 42(7): 3114-3126.

Yang, H., T. An, G. Li, W. Song, W.J. Cooper, H. Luo and X. Guo, 2010. Photocatalytic degradation kinetics and mechanism of environmental pharmaceuticals in aqueous suspension of TiO_2: A case of β-blockers. Journal of Hazardous Materials 179(1-3): 834-839.

8 GLOSSARY

8.1 Definitions

Advanced Oxidation Processes (AOPs)

Advanced Oxidation Processes (AOPs) are based on reactions that utilize powerful oxidizing intermediates (e.g., the hydroxyl radical ·OH) to oxidize primarily organic pollutants from contaminated air and water. The term 'advanced' is used because the chemical reactions involved are essentially the same (except billions of times faster) as those that take place very slowly if these organic pollutants are dispersed into the air or water.

Amphiphile/Amphiphilic

A chemical compound possessing both hydrophilic (water-loving, polar) and hydrophobic (non-polar) characteristics.

Anatase

Anatase is one of the three mineral forms of titanium dioxide (TiO_2).

Band Gap

The band gap of a semiconductor is the minimum energy required to excite an electron that is stuck in its bound state into a free state where it can participate in conduction.

Conduction Band

The energy level at which an electron can be considered free.

Fluence

The flux (radiative power) of the all wavelengths (of light) passing from all directions through a very small sphere over time.

Hydrosilylation

The addition of Si-H (silicon – hydrogen) bonds across unsaturated bonds (e.g., alkenes, alkynes, etc.).

Intercalation

Reversible inclusion of a molecule (or group) between two other molecules (or groups).

Magnesiothermic

A process in which magnesium (Mg) is used to reduce a compound at elevated temperature.

Moiety(ies)

A part or functional group of a molecule.

Nanocomposite

A two phase material that contains nanomaterials as fillers or reinforcement.

Nanocrystal

A solid particle that is a single crystal in the nanometer size range.

Nanoparticle

A solid particle or a material that has at least one dimension in the range of 1 to 100 nm.

Nanosponge

A highly porous material which is composed of nanoparticles.

Photocatalysis

A reaction which uses light to activate a substance which modifies the rate of a chemical reaction without being involved itself.

Photocatalyst

A chemical compound or substance that can modify the rate of a chemical reaction using light irradiation.

Photoexcitation

The process of electron excitation by light (photon) absorption.

Photoinduced

Any process caused by absorption of light.

Photoluminescence

Light emission from any form of matter after the absorption of light (photon).

Scavenger

A substance added to a mixture to remove or inactivate impurities.

Tunability

The ability to tune or control properties of a material.

Valence Band (VB) Electron

The electrons present in the valence band (ground state).

Valence Band Hole

The hole (an empty state) created in the valence band after the electron jumps from valence band to the conduction band.

8.2 Acronyms

AOP	Advanced Oxidation Processes
ca.	circa (about)
CB	Conduction Band
ENPs/NPs	Engineered Nanoparticles/Nanoparticles
eV	Electron Volt
FT-IR	Fourier-Transform Infrared Spectroscopy
IR	Infrared
LC-MS	Liquid Chromatography – Mass Spectrometry
MS	Mass Spectrometry
NC	Nanocrystal
NPs	Nanoparticles
OSPW	Oil Sands Process Water
OSRIN	Oil Sands Research and Information Network
PL	Photoluminescence
QY/QYs	Quantum Yield/s
ROS	Reactive Oxygen Species
SEE	School of Energy and the Environment
SEM	Scanning Electron Microscopy
TEM	Transmission Electron Microscopy
UV	Ultraviolet
VB	Valence Band
XPS	X-ray Photoelectron Spectroscopy
XRD	X-ray Diffraction

8.3 Chemicals/Chemistry

Ar	Argon
CHA	Cyclohexanoic Acid
DDL	diacetyl-dihydro-lutidine
H_2O_2	Hydrogen Peroxide
HF	Hydrofluoric Acid
$HO_2^{\bullet}$	Hydroperoxyl radical
HSQ	Hydrogen Silsesquioxane
Mg/L	Miligrams per litre
mM	Millimolar
NA / NAs	Naphthenic Acid / Naphthenic Acids
$^{\bullet}OH$	Hydroxyl radical
$^1O_2$	Singlet oxygen
$O_2^{\bullet-}$	Superoxide
Si	Silicon
TiO_2	Titanium dioxide

LIST OF OSRIN REPORTS

OSRIN reports are available on the University of Alberta's Education & Research Archive at http://hdl.handle.net/10402/era.17209. The Technical Report (TR) series documents results of OSRIN funded projects. The Staff Reports (SR) series represent work done by OSRIN staff.

OSRIN Technical Reports – http://hdl.handle.net/10402/era.17507

BGC Engineering Inc., 2010. Oil Sands Tailings Technology Review. OSRIN Report No. TR-1. 136 pp. http://hdl.handle.net/10402/era.17555

BGC Engineering Inc., 2010. Review of Reclamation Options for Oil Sands Tailings Substrates. OSRIN Report No. TR-2. 59 pp. http://hdl.handle.net/10402/era.17547

Chapman, K.J. and S.B. Das, 2010. Survey of Albertans' Value Drivers Regarding Oil Sands Development and Reclamation. OSRIN Report TR-3. 13 pp. http://hdl.handle.net/10402/era.17584

Jones, R.K. and D. Forrest, 2010. Oil Sands Mining Reclamation Challenge Dialogue – Report and Appendices. OSRIN Report No. TR-4. 258 pp. http://hdl.handle.net/10402/era.19092

Jones, R.K. and D. Forrest, 2010. Oil Sands Mining Reclamation Challenge Dialogue – Report. OSRIN Report No. TR-4A. 18 pp. http://hdl.handle.net/10402/era.19091

James, D.R. and T. Vold, 2010. Establishing a World Class Public Information and Reporting System for Ecosystems in the Oil Sands Region – Report and Appendices. OSRIN Report No. TR-5. 189 pp. http://hdl.handle.net/10402/era.19093

James, D.R. and T. Vold, 2010. Establishing a World Class Public Information and Reporting System for Ecosystems in the Oil Sands Region – Report. OSRIN Report No. TR-5A. 31 pp. http://hdl.handle.net/10402/era.19094

Lott, E.O. and R.K. Jones, 2010. Review of Four Major Environmental Effects Monitoring Programs in the Oil Sands Region. OSRIN Report No. TR-6. 114 pp. http://hdl.handle.net/10402/65.20287

Godwalt, C., P. Kotecha and C. Aumann, 2010. Oil Sands Tailings Management Project. OSRIN Report No. TR-7. 64 pp. http://hdl.handle.net/10402/era.22536

Welham, C., 2010. Oil Sands Terrestrial Habitat and Risk Modeling for Disturbance and Reclamation – Phase I Report. OSRIN Report No. TR-8. 109 pp. http://hdl.handle.net/10402/era.22567

Schneider, T., 2011. Accounting for Environmental Liabilities under International Financial Reporting Standards. OSRIN Report TR-9. 16 pp. http://hdl.handle.net/10402/era.22741

Davies, J. and B. Eaton, 2011. Community Level Physiological Profiling for Monitoring Oil Sands Impacts. OSRIN Report No. TR-10. 44 pp. http://hdl.handle.net/10402/era.22781

Hurndall, B.J., N.R. Morgenstern, A. Kupper and J. Sobkowicz, 2011. Report and Recommendations of the Task Force on Tree and Shrub Planting on Active Oil Sands Tailings Dams. OSRIN Report No. TR-11. 15 pp. http://hdl.handle.net/10402/era.22782

Gibson, J.J., S.J. Birks, M. Moncur, Y. Yi, K. Tattrie, S. Jasechko, K. Richardson, and P. Eby, 2011. Isotopic and Geochemical Tracers for Fingerprinting Process-Affected Waters in the Oil Sands Industry: A Pilot Study. OSRIN Report No. TR-12. 109 pp. http://hdl.handle.net/10402/era.23000

Oil Sands Research and Information Network, 2011. Equivalent Land Capability Workshop Summary Notes. OSRIN Report TR-13. 83 pp. http://hdl.handle.net/10402/era.23385

Kindzierski, W., J. Jin and M. Gamal El-Din, 2011. Plain Language Explanation of Human Health Risk Assessment. OSRIN Report TR-14. 37 pp. http://hdl.handle.net/10402/era.23487

Welham, C. and B. Seely, 2011. Oil Sands Terrestrial Habitat and Risk Modelling for Disturbance and Reclamation – Phase II Report. OSRIN Report No. TR-15. 93 pp. http://hdl.handle.net/10402/era.24547

Morton Sr., M., A. Mullick, J. Nelson and W. Thornton, 2011. Factors to Consider in Estimating Oil Sands Plant Decommissioning Costs. OSRIN Report No. TR-16. 62 pp. http://hdl.handle.net/10402/era.24630

Paskey, J. and G. Steward, 2012. The Alberta Oil Sands, Journalists, and Their Sources. OSRIN Report No. TR-17. 33 pp. http://hdl.handle.net/10402/era.25266

Cruz-Martinez, L. and J.E.G. Smits, 2012. Potential to Use Animals as Monitors of Ecosystem Health in the Oil Sands Region – July 2013 Update. OSRIN Report No. TR-18. 59 pp. http://hdl.handle.net/10402/era.25417

Hashisho, Z., C.C. Small and G. Morshed, 2012. Review of Technologies for the Characterization and Monitoring of VOCs, Reduced Sulphur Compounds and CH_4. OSRIN Report No. TR-19. 93 pp. http://hdl.handle.net/10402/era.25522

Kindzierski, W., J. Jin and M. Gamal El-Din, 2012. Review of Health Effects of Naphthenic Acids: Data Gaps and Implications for Understanding Human Health Risk. OSRIN Report No. TR-20. 43 pp. http://hdl.handle.net/10402/era.26060

Zhao, B., R. Currie and H. Mian, 2012. Catalogue of Analytical Methods for Naphthenic Acids Related to Oil Sands Operations. OSRIN Report No. TR-21. 65 pp. http://hdl.handle.net/10402/era.26792

Oil Sands Research and Information Network and Canadian Environmental Assessment Agency, 2012. Summary of the Oil Sands Groundwater – Surface Water Interactions Workshop. OSRIN Report No. TR-22. 125 pp. http://hdl.handle.net/10402/era.26831

Valera, E. and C.B. Powter, 2012. Implications of Changing Environmental Requirements on Oil Sands Royalties. OSRIN Report No. TR-23. 21 pp. http://hdl.handle.net/10402/era.27344

Dixon, R., M. Maier, A. Sandilya and T. Schneider, 2012. Qualifying Environmental Trusts as Financial Security for Oil Sands Reclamation Liabilities. OSRIN Report No. TR-24. 32 pp. http://hdl.handle.net/10402/era.28305

Creasey, R., 2012. Workshop on the Information that Professionals Would Look for in Mineable Oil Sands Reclamation Certification. OSRIN Report No. TR-25. 52 pp. http://hdl.handle.net/10402/era.28331

Alberta Innovates – Technology Futures, 2012. Investigating a Knowledge Exchange Network for the Reclamation Community. OSRIN Report No. TR-26. 42 pp. http://hdl.handle.net/10402/era.28407

Dixon, R.J., J. Kenney and A.C. Sandilya, 2012. Audit Protocol for the Mine Financial Security Program. OSRIN Report No. TR-27. 27 pp. http://hdl.handle.net/10402/era.28514

Davies, J., B. Eaton and D. Humphries, 2012. Microcosm Evaluation of Community Level Physiological Profiling in Oil Sands Process Affected Water. OSRIN Report No. TR-28. 33 pp. http://hdl.handle.net/10402/era.29322

Thibault, B., 2012. Assessing Corporate Certification as Impetus for Accurate Reporting in Self-Reported Financial Estimates Underlying Alberta's Mine Financial Security Program. OSRIN Report No. TR-29. 37 pp. http://hdl.handle.net/10402/era.29361

Pyper, M.P., C.B. Powter and T. Vinge, 2013. Summary of Resiliency of Reclaimed Boreal Forest Landscapes Seminar. OSRIN Report No. TR-30. 131 pp. http://hdl.handle.net/10402/era.30360

Pyper, M. and T. Vinge, 2013. A Visual Guide to Handling Woody Materials for Forested Land Reclamation. OSRIN Report No. TR-31. 10 pp. http://hdl.handle.net/10402/era.30381

Mian, H., N. Fassina, A. Mukherjee, A. Fair and C.B. Powter, 2013. Summary of 2013 Tailings Technology Development and Commercialization Workshop. OSRIN Report No. TR-32. 69 pp. http://hdl.handle.net/10402/era.31012

Howlett, M. and J. Craft, 2013. Application of Federal Legislation to Alberta's Mineable Oil Sands. OSRIN Report No. TR-33. 94 pp. http://hdl.handle.net/10402/era.31627

Welham, C., 2013. Factors Affecting Ecological Resilience of Reclaimed Oil Sands Uplands. OSRIN Report No. TR-34. 44 pp. http://hdl.handle.net/10402/era.31714

Naeth, M.A., S.R. Wilkinson, D.D. Mackenzie, H.A. Archibald and C.B. Powter, 2013. Potential of LFH Mineral Soil Mixes for Land Reclamation in Alberta. OSRIN Report No. TR-35. 64 pp. http://hdl.handle.net/10402/era.31855

Welham, C. and B. Seely, 2013. Oil Sands Terrestrial Habitat and Risk Modelling for Disturbance and Reclamation: The Impact of Climate Change on Tree Regeneration and Productivity – Phase III Report. OSRIN Report No. TR-36. 65 pp. http://hdl.handle.net/10402/era.31900

Eaton, B., T. Muhly, J. Fisher and S-L. Chai, 2013. Potential Impacts of Beaver on Oil Sands Reclamation Success – an Analysis of Available Literature. OSRIN Report No. TR-37. 65 pp. http://hdl.handle.net/10402/era.32764

Paskey, J., G. Steward and A. Williams, 2013. The Alberta Oil Sands Then and Now: An Investigation of the Economic, Environmental and Social Discourses Across Four Decades. OSRIN Report No. TR-38. 108 pp. http://hdl.handle.net/10402/era.32845

Watson, B.M. and G. Putz, 2013. Preliminary Watershed Hydrology Model for Reclaimed Oil Sands Sites. OSRIN Report No. TR-39. 193 pp. http://hdl.handle.net/10402/era.34250

Birks, S.J., Y. Yi, S. Cho, J.J. Gibson and R. Hazewinkel, 2013. Characterizing the Organic Composition of Snow and Surface Water in the Athabasca Region. OSRIN Report No. TR-40. 62 pp. http://hdl.handle.net/10402/era.36643

De Corby, R.G., 2013. Development of Silicon-Based Optofluidic Sensors for Oil Sands Environmental Monitoring. OSRIN Report No. TR-41. 19 pp. http://hdl.handle.net/10402/era.36936

OSRIN Videos – http://hdl.handle.net/10402/era.29304

Rooney Productions, 2012. Assessment Methods for Oil Sands Reclamation Marshes. OSRIN Video No. V-1. 20 minutes. Also available on the University of Alberta You Tube Channel (recommended approach).

Rooney Productions, 2012. Assessment Methods for Oil Sands Reclamation Marshes. OSRIN Video No. V-1. Nine-part mobile device version. Also available on the University of Alberta You Tube Channel (link to Part 1 - recommended approach).

OSRIN Staff Reports – http://hdl.handle.net/10402/era.19095

OSRIN, 2010. Glossary of Terms and Acronyms used in Oil Sands Mining, Processing and Environmental Management - January 2013 Update. OSRIN Report No. SR-1. 119 pp. http://hdl.handle.net/10402/era.17544

OSRIN, 2010. OSRIN Writer's Style Guide – November 2013 Update. OSRIN Report No. SR-2. 29 pp. http://hdl.handle.net/10402/era.17545

OSRIN, 2010. OSRIN Annual Report: 2009/2010. OSRIN Report No. SR-3. 27 pp. http://hdl.handle.net/10402/era.17546

OSRIN, 2010. Guide to OSRIN Research Grants and Services Agreements - June 2011 Update. OSRIN Report No. SR-4. 21 pp. http://hdl.handle.net/10402/era.17558

OSRIN, 2011. Summary of OSRIN Projects – June 2013 Update. OSRIN Report No. SR-5. 81 pp. http://hdl.handle.net/10402/era.20529

OSRIN, 2011. OSRIN Annual Report: 2010/11. OSRIN Report No. SR-6. 34 pp. http://hdl.handle.net/10402/era.23032

OSRIN, 2011. OSRIN's Design and Implementation Strategy. OSRIN Report No. SR-7. 10 pp. http://hdl.handle.net/10402/era.23574

OSRIN, 2012. OSRIN Annual Report: 2011/12. OSRIN Report No. SR-8. 25 pp. http://hdl.handle.net/10402/era.26715

OSRIN, 2013. OSRIN Annual Report: 2012/13. OSRIN Report No. SR-9. 56 pp. http://hdl.handle.net/10402/era.31211